

## Luminescence performance of Cerium(III) ions incorporated into organofunctional mesoporous silica

Natalia G. Kobylinska <sup>a</sup>, Oksana A. Dudarko <sup>b\*</sup>, Inna V. Melnyk <sup>b</sup>, Gulaim A. Seisenbaeva <sup>c</sup>, Vadim G. Kessler <sup>c</sup>

<sup>a</sup> Faculty of Chemistry, Taras Shevchenko National University of Kyiv, 64/13 Volodymyrska Str., Kyiv, 01601, Ukraine

<sup>b</sup> Chuiko Institute of Surface Chemistry, NAS of Ukraine, 17 General Naumov Str., Kyiv, 03164, Ukraine

<sup>c</sup> Department of Chemistry, Swedish University of Agricultural Sciences, 750 07, Uppsala, Sweden



### ARTICLE INFO

#### Keywords:

Rare-earth elements (REEs), photoluminophores  
Ordered silica  
Phosphonic groups  
Phenylsulfonic (or benzenesulfonic) groups

### ABSTRACT

Series of SBA-15 derived ordered mesoporous silica adsorbents bearing phenylsulfonic, phosphonic groups and their combinations were synthesized by non-grafting approach. Sodium metasilicate was used as precursor for the silica matrix. The materials were characterized using <sup>1</sup>H, <sup>31</sup>P, <sup>29</sup>Si and <sup>13</sup>C solid-state NMR spectroscopy, N<sub>2</sub>-physisorption isotherms, powder XRD, FTIR, TGA, SEM and TEM. It was found that all the samples exhibited typical hexagonal arrangement of mesoporous structure with high surface area. The active organic functions were, at least to some extent, incorporated into the framework of SBA-15, efficiently promoting the uptake of Ce (III) into the produced SBA-15 type matrices. Significant changes in luminescence of the samples were observed with both increasing content of incorporated cation and with change of heteroatoms (O, P, S) in functional groups of silica. The shapes of the peaks at 350–360 nm in the photoluminescence spectra originating from the 4f→5d (<sup>2</sup>F<sub>5/2</sub>, <sup>2</sup>F<sub>7/2</sub>) transitions were indicative of the presence of Ce(III) ions in the mesoporous silica matrix with adsorption capacity increasing in the series up to ~2 mmol·g<sup>-1</sup>(259.2 mg·g<sup>-1</sup>). The Ce-incorporated samples dehydrated in vacuum exhibited decreased photoluminescence with integrated intensities comparable to those of water-containing samples. The high luminescent performances of these luminescent Ce-incorporated mesoporous materials could render attractive potential applications in optical amplification and laser systems, etc.

### 1. Introduction

Rare-earth elements (REEs) are recognized as critical elements in a variety of modern applications such as electronics, catalysis, high-performance magnets, superconductors, telecommunication systems [1], biological assays [2], medical imaging purposes [3] etc. attributing to their unique characteristics. In turn, these elements have always played a prominent role in lighting and light conversion technologies (Auer mantles, incandescent lamps, lasers) and more recently in both cathode-ray [4] and plasma displays. In addition, luminescent REEs have been utilized in lasers, the most important and famous of these being the Nd:YAG system, while many other REEs have been shown to offer laser effects under the proper circumstances [5].

In recent years, much interest has emerged in the Ce(III) ion for its application in high energy physics, because of fast and efficient luminescence in the UV and blue spectral region. The emission of the Ce(III)

ions produced by the 4f-5d electron transition, can be blue/red shifted depending on the type of co-doping in solids [6,7]. Among various inorganic crystalline compositions, Ce<sup>3+</sup>-doped crystals, such as Ce: Y<sub>3</sub>Al<sub>5</sub>O<sub>12</sub> [8], Ce:YAlO<sub>3</sub> [9], Ce: Lu<sub>2</sub>SiO<sub>5</sub> [10] and Ce:Lu<sub>3</sub>Al<sub>5</sub>O<sub>12</sub> [11], have been widely studied for their fast scintillation and high light yield, and good mechanical and chemical stability. To enhance the luminescence performance of Tb(III)-doped inorganic phosphors, co-doping with Ce(III) is an attractive option [12]. Cerium(III) shows intense absorption in the ultraviolet region, and the excitation energy can be transferred to the energy levels of terbium(III). Amorphous silica has been investigated as an alternative to crystalline hosts for X-ray scintillators because of its advantageous mechanical properties (e.g. fibre), its chemical stability and non-hygroscopic nature, the possibility of incorporating larger amounts of luminescent ions [13] and the opportunity of cost reduction [14]. Thus, in last decades, there has been a strong interest in REE-containing organic-inorganic hybrid materials

\* Corresponding author.

E-mail address: [odudarko80@gmail.com](mailto:odudarko80@gmail.com) (O.A. Dudarko).

and cerium as well [15]. In these materials, a molecular REEs complex is embedded in an inorganic host matrix (like the sol-gel-derived materials), or alternatively, an inorganic REEs is embedded in an organic matrix. In early paper, Rand et al. [16] studied the luminescence of un-annealed Ce-doped xerogels of  $\text{SiO}_2$  and found a single emission at 355 nm with the corresponding excitation spectrum peak at 254 nm. In a series of papers Cai et al. [17,18] first prepared and annealed non-doped silica xerogels, and then soaked these in  $\text{Ce}(\text{SO}_4)_2$  or  $\text{CeCl}_3$  solutions or a Ce-containing sol, after which they were dried. In all cases, the luminescence had an emission band around 350 nm. Xu et al. [19] reported that a short wavelength emission near 357 nm occurred for samples processed at temperatures up to about 450 °C, but at higher temperatures above 700 °C this emission was replaced by a band at 450 nm when the Ce (III) ions become coordinated with an oxygen ions. The sol-gel process provides an attractive low temperature alternative to the melt process for producing REEs-doped silica and several reports have been published on the properties of this materials [20].

In the literature, two main luminescent bands of Ce(III) ions at 355–370 nm and 420–450 nm are mentioned for the samples of Ce(III)-doped glasses [19]. Both of the two bands were attributed to the 4f-5d transitions of Ce(III). There is still no doubtless conclusion about the relationship between the luminescence bands and the structure of the coordination environment. In some Ce-doped materials, there was only one luminescence band with the maximum at 357 nm [21], but in other samples luminescence bands at 420–450 nm appeared [22]. The luminescence of Ce-doped silica is influenced by factors such as modification of the ligand field around the Ce(III) ions in  $\text{SiO}_2$ , presence of hydroxide ions, energy transfer by cross relaxation and the concentration of dopants. It was therefore of great interest to distinguish between the luminescence arising from Ce(III) ions and of that arising from defect centers in the silica.

The solid matrixes bearing functional groups capable to bind REEs in a monolayer with well-defined coordination on the surface, have recently been shown to induce luminescence due to electron transitions in the REE centers enhanced by the interaction silica nanoparticles with functional groups [23]. The application of mesoporous silica such as SBA-15 as a matrix for producing REEs-doped materials has different advantages compared to glass materials or dense silica nanoparticles, among them the high chemical and thermal stability [24], large surface area, ordered pore structure, etc [25]. It has been demonstrated that Ce (III) can be doped within mesoporous silica pores by various methods [17,26,27]. Firstly, the technique is based on the introduction of Ce(III) ions on the outer surface of the SBA-15 pores by physical adsorption [28]. Secondly, the technique is based on ion-exchange with surface functional groups. In the work [28] functionalization of the ordered mesoporous silica SBA-15 was realized by depositing on its surface a layer of phosphorus  $\text{CeF}_3 \cdot \text{Eu}^{3+}$  using three different methods, such as *in situ* reaction, solution impregnation and solid phase grinding synthesis, respectively. The authors proved that efficient energy transfer in the mesoporous material mainly carried out between the REE ions. It was found that the obtained samples, if using different synthesis methods showed different luminescence properties, related to the guest-host interactions between the guest molecule and the silica matrix. Also, other factors such as modification of the ligand field around the  $\text{Ce}^{3+}$  ions in silica, presence of hydroxide ions, energy transfer by cross-relaxation and the concentration of the co-dopants have significant effect on the luminescent wavelength and intensity.

In our previous work we have already demonstrated that the silica gel modified with propyl sulfonic groups significantly increased the luminescence intensity of REEs [29]. The Klier K. et al., in 2008 [30] studied interaction of Ce(III) ions in ~0.5 mEq/g amount with SBA-15 matrix modified with propyl sulfonic groups with a monovalent cation exchange capacity of ~1 mEq/g. The high surface concentration of the sulfonic groups affords target sites that were essential for the formation of the Ce(III) complexes. The obtained Ce-containing material was displaying high intensity purple photoluminescence. Probably, replacing

the propyl sulfonic group with phenyl sulfonic intensified the bond of the sulfonic group with REEs. Thus, the combination of phenyl and sulfonic groups would be capable to enhance the interaction of sulfonic groups with REEs [28], potentially opening for obtaining highly efficient luminophores. Mesoporous silica functionalized with sulfonic groups has the advantage of its high acid strength and an adjustable acid group density that allows rapid proton transport via channels [31]. Although, insignificant effect was observed for interaction of REEs with silica modified with phenyl groups alone [24]. It should be noted the abundance of reports on luminescence of REEs in mesoporous materials [25, 27], but the polyfunctional mesoporous silica have not been investigated to any comparable extent with respect to photoluminescence.

Usually, the synthesis of SBA-15 silica matrixes is based on the hydrolysis and condensation of tetraethylorthosilicate (TEOS) under acidic or basic conditions [32]. TEOS is expensive reagent and the produced silica is costly. Thus, using sodium metasilicate as precursor for synthesis SBA-15 would render mesoporous silica more economically sustainable [33]. This was our main consideration for the selection of  $\text{Na}_2\text{SiO}_3$  as precursor for this study.

In this work, the primary goal was to synthesize new mono- and bifunctional mesoporous materials with various combinations of phenyl (-Ph), sulfonic (- $\text{SO}_3\text{H}$ ), phenylsulfonic (- $\text{PhSO}_3\text{H}$ ) and phosphonic (-P (O)(OH)<sub>2</sub>) groups using template method. The second motivation was to investigate in detail the effect of amount and nature of heteroatoms (O, P, S) in functional groups of silica on the Ce-incorporation evaluating their photoluminescence properties. Ce (III) was chosen as the most abundant rare-earth metal, and the most reactive among them (except for europium). As materials bearing sulphonate and phosphonic groups with Ce(III) were studied, we expected synergistic effect to be created by the presence of functional groups combination on the pore surface of SBA-15 carriers. The organofunctional mesoporous materials were obtained and their adsorbent characteristics towards Ce(III) as well as photoluminescence properties of materials resulting from its surface complexation were investigated. It is known that the presence of moist air could influence the photoluminescence properties of Ce(III)-containing compounds, therefore the differences of emission bands between the hydrated and vacuum-dried Ce-incorporated SBA-15-based materials were examined. Developed and investigated Ce-incorporating silicas can find potential applications as catalysts, energy storages, adsorbents for pollutants in remediation technologies, and nanoelectronics devices.

## 2. Experimental part

### 2.1. Reagents

Sodium metasilicate,  $\text{Na}_2\text{SiO}_3 \cdot 5\text{H}_2\text{O}$  (SS, Sigma, USA); diethylphosphatoethyltriethoxysilane,  $\text{C}_{12}\text{H}_{29}\text{O}_6\text{PSi}$  (DPTS, 98%, Gelest); phenyltriethoxysilane,  $\text{C}_{12}\text{H}_{20}\text{O}_3\text{Si}$  (PhTES, 99%, Gelest), chlorosulfonic acid ( $\text{ClSO}_3\text{H}$ , 99%, Sigma-Aldrich), pluronic P123 (copolymer: polyethylene - polypropylene - polyethylene glycol,  $\text{EO}_{20}\text{RO}_{70}\text{EO}_{20}$ , P123, 99%, BASF, USA), concentrated hydrochloric acid, concentrated sulfuric acid, ethanol (abs.).  $\text{CeCl}_3 \cdot 7\text{H}_2\text{O}$  (99%, CAS 18618-55-8, Ourchem), Varian bond phenylsulfonic (or benzenesulfonic) Elut SCX sorbent (named as **VPhSOH**), sodium hydroxide (pellets for analysis, MERCK), potassium chloride (0.1 mol·L<sup>-1</sup> standard).

The Ce(III) stock solution was prepared by dissolving the appropriate amounts of  $\text{CeCl}_3 \cdot 7\text{H}_2\text{O}$  in water without acid. All other chemicals were of analytical grade and used without further purification. Deionized water used in all experiments was obtained from the Milli-Q water purification system.

## 2.2. Synthesis of mesoporous silica samples

### 2.2.1. Synthesis of monofunctional phenyl-containing SBA-15 (**Ph**) was performed by a modified method [34]

4 g of P123 was dissolved in 40 cm<sup>3</sup> of water with constant stirring. 37 cm<sup>3</sup> of conc. hydrochloric acid was mixed with the resulting clear solution. Then 0.004 mol of PhTES was added and stirred for 5 h (turbid solution). The obtained sol was heated at 50 °C for 1 h. Separately, 0.04 mol of SS in 40 cm<sup>3</sup> of water were dissolved, the resulting solution was added to the acidified solution of the template with silane and was stirred at 50 °C for 1 h. The mixture was transferred inside the Teflon tube and the hydrothermal treatment (HTT) was performed at 80 °C for 20 h. After HTT, the white precipitate was filtered off and air-dried. Template was removed by boiling in acidified ethanol for 3 h (30 cm<sup>3</sup> ethanol per 1 g of mesophase), the operation was repeated 4 times. Then drying in vacuum was performed: 0.5 h at room temperature, 0.5 h at 50 °C, and 3 h at 100 °C.

### 2.2.2. Synthesis of bifunctional phenyl-containing SBA-15 (**PhP**)

5 g of Pluronic P123 was dissolved in 50 cm<sup>3</sup> of water with constant stirring. 41 cm<sup>3</sup> of conc. hydrochloric acid was added to the resulting clear solution. Then 0.005 mol of PhTES and 0.005 mol of DPTS, were mixed for 0.5 h (turbid solution). 0.05 mol of SS in 50 cm<sup>3</sup> of water were separately dissolved, the resulting solution was added to the acidified solution of the template with silanes.

### 2.2.3. Synthesis of bifunctional phosphonic- and phenyl-containing SBA-15 (**PhPOH-1**)

2 g of the sample **PhP** was mixed with 20 cm<sup>3</sup> of conc. hydrochloric acid and hydrolyzed for 5 h at 65°C and then 2 h at 80°C in the oven without stirring. The resulted precipitate was washed with distilled water till pH 6. Then, sample was dried step-by-step: 0.5 h at room temperature, 0.5 h at 50 °C, and 3 h at 100 °C in vacuum. The reaction pathway is presented in [Scheme 1](#).

### 2.2.4. Synthesis of bifunctional phosphonic- and phenylsulfonic-containing SBA-15 (**PhSOHPOH-1**)

Sulfonation of the phenyl group was carried out with chlorosulfonic acid in the presence of CH<sub>2</sub>Cl<sub>2</sub> under reflux for 1 h (25 cm<sup>3</sup> of CH<sub>2</sub>Cl<sub>2</sub>, 5.2 cm<sup>3</sup> of ClSO<sub>3</sub>H, 1.5 g of phenyl-functional material). After the reaction for removing unreacted chlorosulfonic acid the product was washed with water. Then washed with 100 cm<sup>3</sup> of H<sub>2</sub>O-THF (1: 1), a mixture of (II), 100 cm<sup>3</sup> of THF, (III), 100 cm<sup>3</sup> of diethyl ether and finally the material was dried in vacuum (393 K, 3 h). Thus, the **Ph** sample was transferred to derivate (named as **PhSOH**) according to [Scheme 1](#) (second step).

### 2.2.5. Synthesis of bifunctional phosphonic- and phenyl-containing SBA-15 (**PhPOH-2**)

The same as **PhP**, but with prehydrolysis of DPTS (1.6 cm<sup>3</sup>) in conc. hydrochloric acid (4.4 cm<sup>3</sup>) for 24 h at 80°C [35]. A schematic

mechanism for the transformation of **PhPOH-2** sample to sulfonic-containing derivate (named as **PhSOHPOH-2**) is analogous to the second step in [Scheme 1](#).

## 2.3. Characterization of mesoporous samples

Scanning Electron Microscopy (SEM) images of the samples were obtained by a JEOL JSM-6060LA (Jeol, Tokyo, Japan) device in the secondary electron mode with accelerating voltage of 30 kV. Transmission electron microscopy (TEM) images of the samples were obtained using a JEM-1230 (JEOL, Japan) instrument. For analysis, the powdery samples were dispersed in ethanol with a moderate ultrasound treatment (22 kHz 30 min) at concentration of ~5 wt % of solids. The diffractograms of the synthesized materials in the region of 0.5–5 2θ° were registered using a DRON-4-07 diffractometer with CuKα radiation.

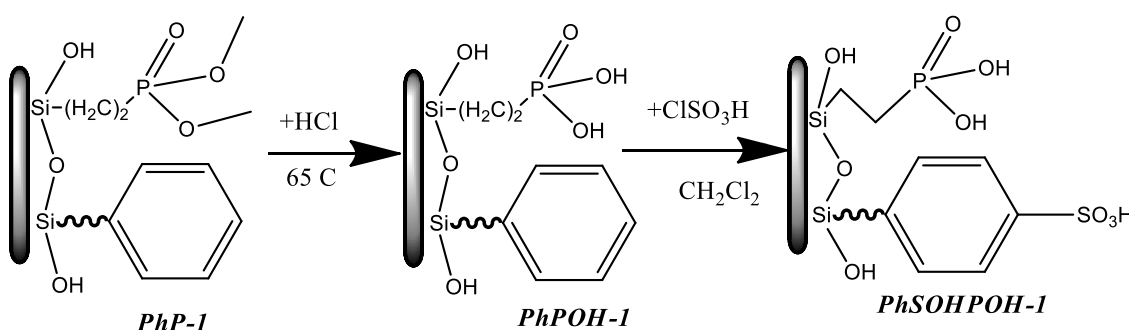
Textural properties of synthesized samples (surface area  $S_{BET}$  and pore-size distribution (PSD)) were evaluated from the nitrogen physical adsorption-desorption isotherms at –196 °C obtained with the KELVIN 1042 (Costech International). Before analysis, samples were dried at 100 °C at least for 1 h in a helium flow. Specific surface area ( $S_{BET}$ ) was evaluated from the nitrogen physical adsorption–desorption isotherms by BET methods in the range of relative pressures  $P/P_0 = 0.05$ –0.20. PSD together with the maximum pore diameters ( $D_{BJH}$ ) were determined by BJH method [36].

FTIR spectra were recorded on a Thermo Nicolet 470 Nexus Fourier-transform infrared spectrometer in the 400–4000 cm<sup>-1</sup> range, using Nexus Smart Collector mode and averaging 50 scans with a resolution of 8 cm<sup>-1</sup>. The silica samples were previously grounded with solid KBr (reagent grade) at a ratio of 1:20.

Room temperature solid state NMR spectra were collected on a Bruker AVANCE III 400WB equipped with a 4-mm MAS probe, operating at <sup>31</sup>P resonance frequency of 161.97 MHz and <sup>13</sup>C resonance frequency of 100.64 MHz. Samples were packed in zirconia rotor with Kel-F tape. The spectra were obtained at a spinning speed of 5–10 kHz.

Potentiometric acid-base titration was used to determine concentration of available acidic functional groups on the surface of silica samples using a standard NaOH solution (0.1–0.05 mol·dm<sup>-3</sup>) after reaching equilibrium. The silica sample (0.05–0.1 g) was added to 0.1 mol·dm<sup>-3</sup> sodium chloride (20 cm<sup>3</sup>) and incubated for 12 h. The titration was executed with the ionmeter ‘I-500’.

The complete thermogravimetric analysis (TGA) of the synthesized substances was performed on a Paulik-Paulik-Erday (Q-1500D) system in the temperature range of 20–1000 °C at a heating rate of 5°/min. The sensitivity of the thermowell was 0.1 mg, the sensitivity of DTA-1/5, DTG-1/5, TG-100. The sample of the substance for analysis was carefully ground in an agate mortar. Full thermal analysis in all cases was carried out in air in open crucibles to ensure complete firing of the organic groups.



**Scheme 1.** Transformations of the cell walls in functional mesoporous silica.

## 2.4. Luminescence measurements

Both solid- and liquid-states fluorescence excitation and emission spectra were recorded on a Perkin-Elmer LS 55 Luminescence Spectrometer. The powder samples of each mesoporous material ( $\approx 0.1$  g) were heaped in the tray, covered with a quartz plate and then the solid-state fluorescence excitation and emission spectra were recorded on a spectrometer with slit width of 10 nm at the ambient temperature. Liquid-state fluorescence excitation and emission spectra of the clear solution of Ce(III) in water were performed on Spectrometer with slit width of 15 nm at the ambient temperature. For emission spectra study, the excitation wavelength of both solid and liquid states was set at 366 nm, as selected from their maximum UV-Vis absorption bands.

## 2.5. Incorporation of Ce(III) experiments

The incorporation of Ce(III) was carried out with 0.4–0.5 g of the mesoporous material with  $20\text{ cm}^3$  of ca.  $0.1\text{ mol}\cdot\text{dm}^{-3}$  aqueous solution of  $\text{CeCl}_3$  at room temperature for 4 h, filtered on circle papers (Whatman®, Grade 2), and washed with distilled water for neutral pH medium. A subsequent thermal treatment of the samples included an overnight drying at  $60^\circ\text{C}$  in air and dehydration at  $110^\circ\text{C}$  under argon atmosphere for 6 h. Each of the prepared silica samples was investigated to the fluorescence measurements.

Batch sorption experiments were carried out in a series of  $25\text{ cm}^3$  glasses containing  $25\text{ cm}^3$  of a  $60\text{ mg}\cdot\text{dm}^{-3}$  solution of Ce(III) ions. Predetermined amounts of adsorbents (0.1 g) were added to the test vessel. All the experiments were performed in the dark in a thermostatically controlled shaker, maintained at 200 rpm and a pre-set temperature of  $25^\circ\text{C}$ . Based on the results from preliminary kinetic studies, a stirring time of 2 h was selected as the equilibrium time for all the sorbents. On completion of the sorption experiments with functionalized silica, the samples were filtered through paper filters to separate the silica particles from the aqueous phase. The metal ion concentration in the filtrate was measured by inductively coupled plasma optical emission spectrometry (ICP-OES) iCAP 6300 (Thermo Scientific, USA).

The adsorption capacity of adsorbents was calculated as the difference between the amount of analyte initially added to the system and the amount remaining in the solution after equilibration using the following equation:

$$q_e(\text{mg}\cdot\text{g}^{-1}) = \frac{(C_0 - C_e)\cdot V}{m} \cdot A_r \quad (1)$$

where,  $q_e$  is the amount of Ce(III) adsorbed per mass unit of adsorbent at equilibrium ( $\text{mg}\cdot\text{g}^{-1}$ );  $C_0$  and  $C_e$  are the initial and equilibrium concentrations of the Ce(III) ions ( $\text{mol}\cdot\text{dm}^{-3}$ ), respectively;  $A_r$  is the atomic weight of the Ce(III) ( $\text{g}\cdot\text{mol}^{-1}$ );  $V$  is the volume of the solution ( $\text{dm}^3$ ); and  $m$  is the weight of the solid (g).

## 3. Results and discussions

### 3.1. Preparation of mesoporous silica samples

The synthesis of mesoporous SBA-15-based materials with covalently immobilized functional groups was performed in a three-step process: 1) mesophase-containing microspheres were synthesized via co-condensation of functional silanes with sodium silicate in the presence of surfactant (e.g. Pluronic 123) often enhancing the condensation via hydrothermal step; 2) the template was removed from the micelles after the porous structure was formed; 3) additional functionality was incorporated either by oxidizing the existing groups or by hydrolysis of ethoxy groups as depicted in Scheme 2.

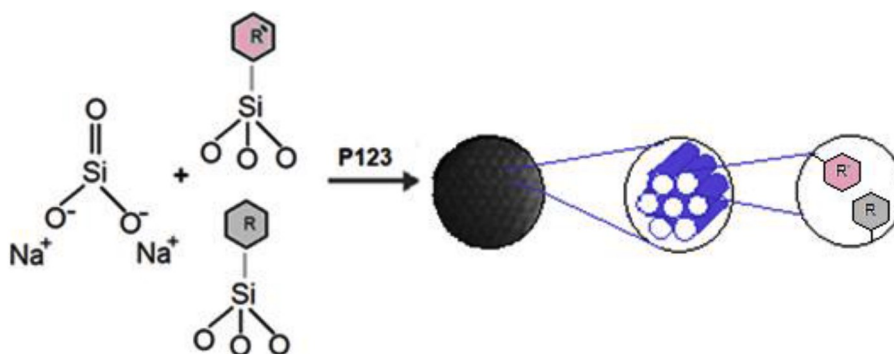
### 3.2. Characterization of mesoporous samples

The morphology of the SBA-15 based samples is shown in Fig. S1. SEM images indicate that the particles modified by phenyl groups of SBA-15 derived from sodium silicate do not have cylindrical shape, otherwise often observed for samples of type SBA-15 synthesized using TEOS as precursor. Depending on the composition of the reaction mixture, the size and shape of the particles differed and agglomerates of size  $1\text{ }\mu\text{m}$  were formed. Agglomeration of materials can be attributed to processes on the surface due to the presence of a high number of phenyl groups. The one-pot synthesis of bifunctional materials with the use of hydrolyzed DPTS is accompanied with the formation of spherical primary particles (*PhP*, *PhPOH-2*). Hydrolysis of phosphate groups with concentrated hydrochloric acid post-synthetically leads to the formation of the structure, as in the case of xerogels [37], but caused the destruction and increase in the mass fraction of amorphous silica.

At the same time, such post-synthetic processing practically does not effect in any way the structural parameters. When comparing the TEM (Fig. 1) photo of all samples, it is obvious that the phenyl groups embedded in the pores do not reduce the structural ordering of the synthesized SBA-15.

The order of porous structure samples was confirmed by TEM images for all samples. As shown in Fig. 1 the hexagonal shape of the mesopores can clearly be observed for the samples either along the pores or perpendicular to the axis of the channels.

The well-ordered mesoporous silica structure was confirmed by small-angle XRD analysis, as shown in Fig. 2, one high-resolved diffraction peak was observed in the small-angle XRD patterns of series phenyl-containing mesoporous silica, which can be assigned to (100) reflections of 2D-hexagonal structures, and is very similar to that of the initial *Ph*. Furthermore, low intensive diffraction peak at  $1.03\text{--}1.05 2\theta$  degree was indicating no significant structure change during the modification process, and these are in good agreement with the results observed from TEM images and  $\text{N}_2$  isotherms. Two diffraction peaks corresponding to the (110) and (200) phases were not observed in the samples due to the presence of the amorphous phase as an impurity.



**Scheme 2.** Preparation of organofunctional silica. R, R' are grafted functional groups (-Ph; -P(O)(OH)<sub>2</sub>; -SO<sub>3</sub>H, -PhSO<sub>3</sub>H).

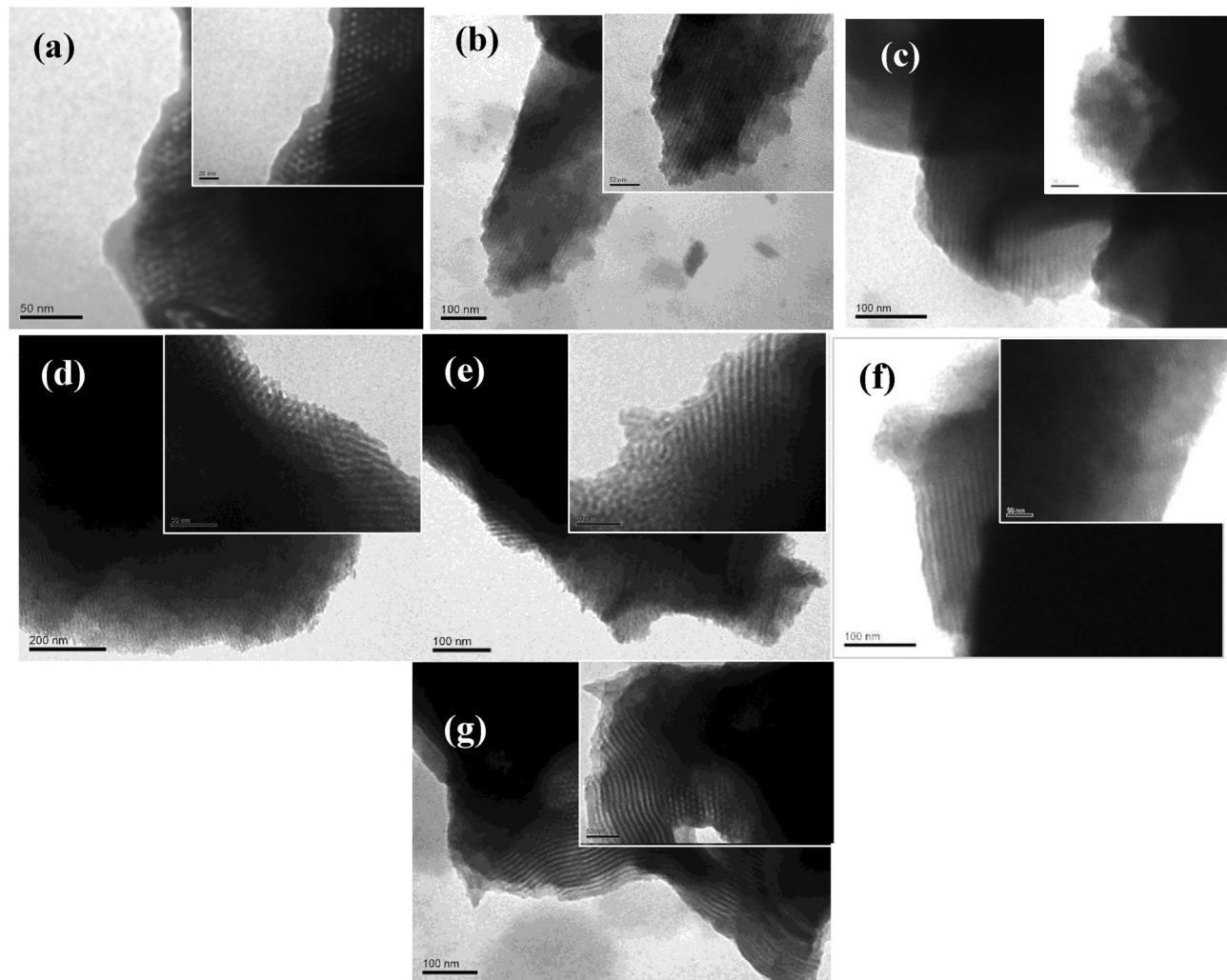


**Fig. 1.** TEM images of functionalized phenyl-containing SBA-15 samples: ***Ph*** (a), ***PhP*** (b), ***PhSOH*** (c), ***PhPOH-1*** (d), ***PhPOH-2*** (e), ***PhSOHPOH-1*** (f), and ***PhSOHPOH-2*** (g).

The surface texture of the materials was investigated by  $N_2$  adsorption-desorption isotherms and pore size distribution curves for all materials (Fig. 3). These isotherms are type IV according to the IUPAC classification [38] and it reveals the well-developed mesoporous structure of the samples (Table 1). The BET surface areas of the samples were calculated and their values are in the range 313–663  $m^2/g$ , the pore diameter of materials according to the BJH model was centered at 3.7–5.6 nm. The size of introduced functional groups effects the porosity parameters. Post-modification with hydrochloric or chlorosulfonic acids decreases the values of specific surface (Table 1, Fig. 3) partially. Acid treatment partially destroys the ordered structure of mesopores and the value of the specific surface area for samples with phosphonic groups decreases (Fig. 3a). Analyzing the desorption curve, we can note that the sample with only hydrophobic phenyl groups ***Ph*** has open mesopores, while due to treatment with sulfonic derivatives, the hysteresis loop shifts to the region of low relative pressures, which indicates the formation of plugged mesopores (Fig. 3b). At the same time, access to the introduced active centers is increasing by enhancement of the pore diameter and sorption volume. Unlike the hydrophobic starting phenyl-containing materials, the samples with sulfonic and phosphonic groups on the surface have greater affinity of the surface to REEs ions, which allows for introduction of cerium(III) cations by chemical interaction rather than physical impregnation of the surface layers.

Analysis of the IR spectra of functionalized silica samples (Fig. S2) allowed identifying the absorption bands characterizing the symmetric

C–H stretching in the range of 2860–2980  $cm^{-1}$  and asymmetric vibrations of the Si–O–Si frame at 1080, 800, and 465  $cm^{-1}$ . Characteristic absorption bands of the phenyl group are observed at 3077, 3055, 1600 and 1430  $cm^{-1}$ . In particular, the bands of the substituted phenyl group also appear at 740 and 700  $cm^{-1}$ . The IR data demonstrate that silane with phenyl groups can be incorporated into the silica framework during such synthesis. Asymmetric stretching vibrations of S=O at 1392  $cm^{-1}$  and symmetric stretching vibrations of S=O from sulfonic acid group at 1214  $cm^{-1}$  in the spectrum of ***PhSOH*** sample confirm the success in phenyl groups sulfonation by the selected method.

Chemical characterization of the surface of bifunctional samples with phosphonic groups and their derivate modified by sulfonic acid, and determination of the structure of functional groups was performed by solid-state NMR spectroscopy (Fig. 4).

In our experiments, the  $^1H$ – $^{29}Si$  CP MAS NMR spectra of silica displayed several peaks (Fig. 4): at –99.1 ppm, at –102.9 ppm and –110.2 ppm. The peaks for both ***PhPOH-2*** and ***PhSOHPOH-2*** samples can be assigned to different Q species i.e. geminal silanols ( $Q_2 = [(HO)_2Si(OSi)_2]$ ;  $\delta = -99.1$  ppm), single silanols ( $Q_3 = [HO-Si(OSi)_3]$ ;  $\delta = -102.9$  ppm), and siloxane groups ( $Q_4 = [Si-(OSi)_4]$ ;  $\delta = -110.2$  ppm). The bifunctional silica and its derivate (***PhSOHPOH-2***) contain different  $T_n$  species ( $1 < n \leq 3$ ) where n is related to the number of siloxane bonds formed between the surface and the functional center at –60.9 and –55.1 ppm that can be assigned to  $T_3$  [ $R-Si-(OSi)_3$ ] and  $T_2$  [ $R_2-Si-(OSi)_2$ ] groups, respectively.

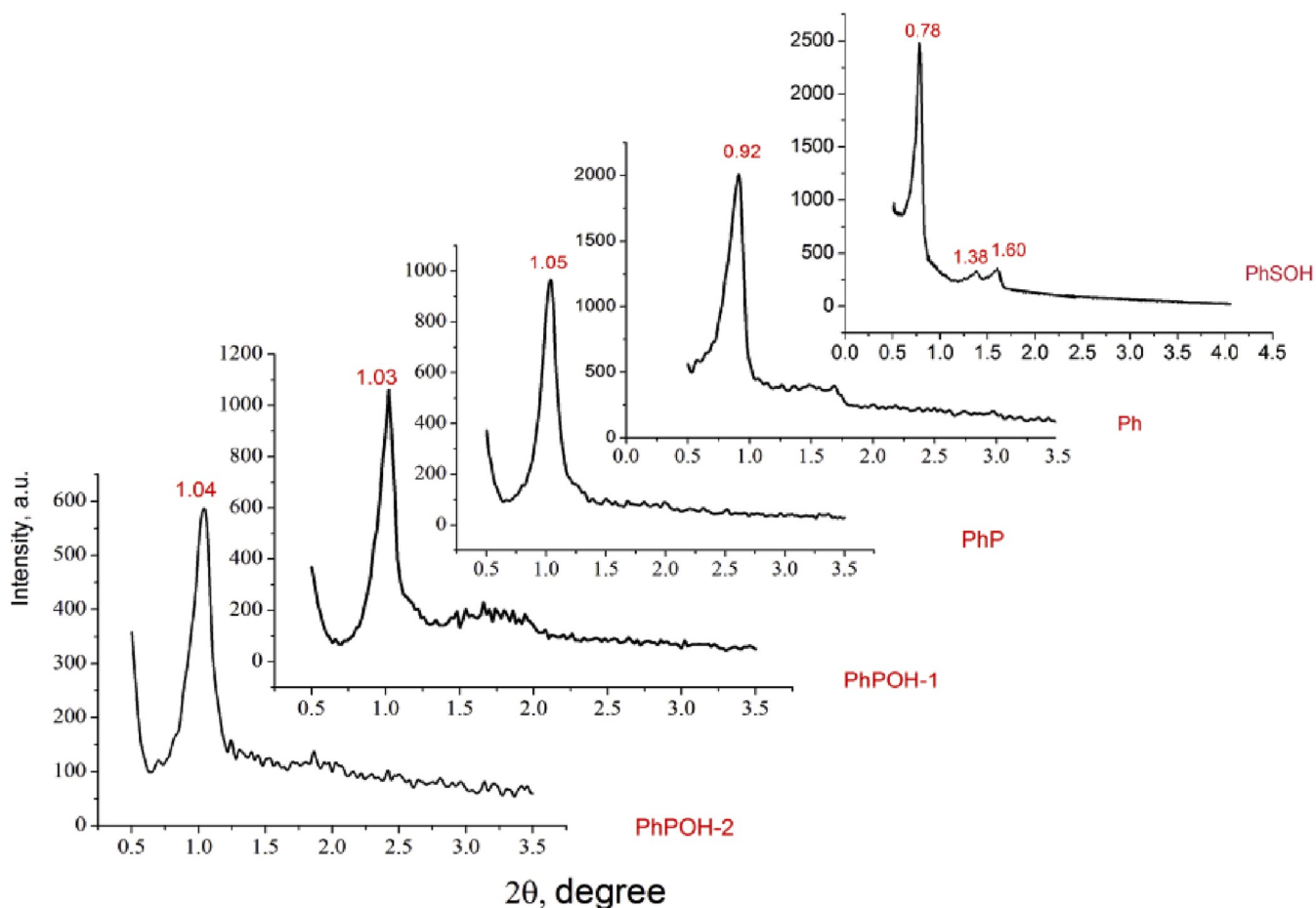


Fig. 2. Small-angle XRD patterns of the obtained phenyl-containing SBA-15 samples.

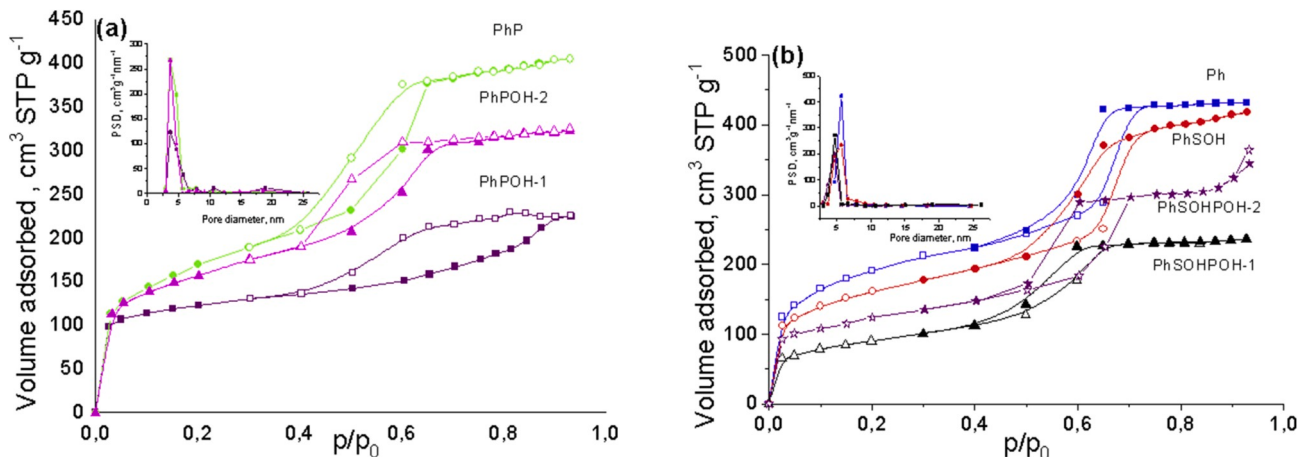


Fig. 3.  $\text{N}_2$  ad/desorption isotherms (a, b) and pore distribution (insert) of mesoporous phenyl-containing samples.

The chemical transformation of the phenyl groups to phenylsulfonic (according to Schema 1) in **PhPOH-2** and its derivative **PhSOHPOH-2** samples was confirmed by  $^{13}\text{C}$  CP MAS NMR spectra. The **PhPOH-2** sample shows chemical shifts for  $^{13}\text{C}$  at 5.1, 16.3, 19.6, 58.8, 70.2, 129.0 and 134.2 ppm which correspond to the aliphatic and aromatic regions of spectra. The peaks at 129.0 and 134.2 ppm in aromatic region are attributed to carbons of benzene ring. The presence of several resolved and overlapping peaks in the aliphatic region indicates the methylene carbon atoms bonded to  $\text{SiO}_2$  matrix and **PhSOHPOH-2** ethoxy groups in  $\text{Si}-\text{O}-\text{CH}_2\text{CH}_3$  (or  $\text{P}-\text{O}-\text{CH}_2\text{CH}_3$ ) groups under synthesis conditions.

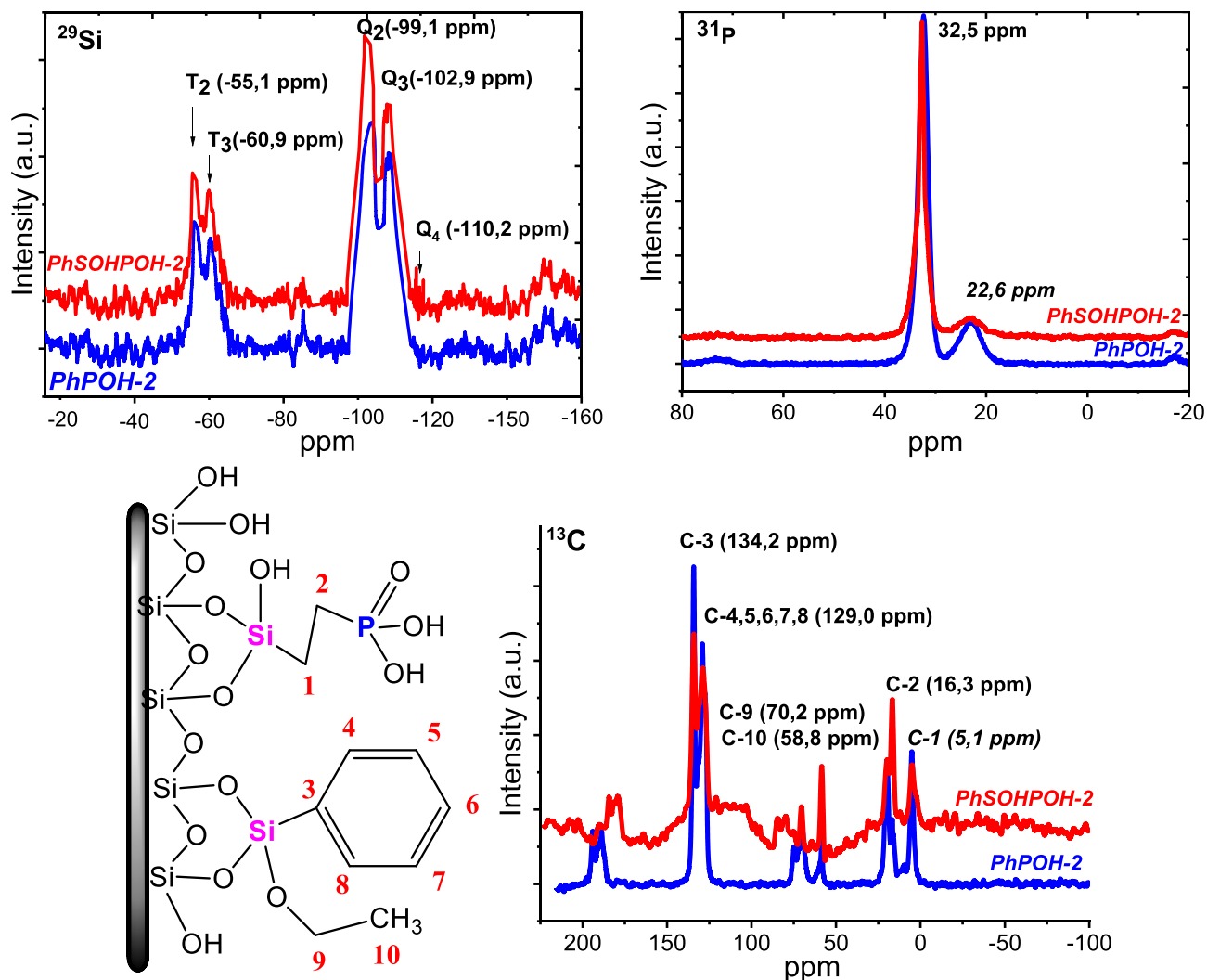
Similarly to the spectrum of **PhPOH-2**, the spectrum of **PhSOHPOH-2** (Fig. 4) contains peaks in the aliphatic and aromatic region, confirming that functional groups remains in the surface after reaction sulfonation, in agreement with Schema 1. The chemical shift is observed in the range of 70–90 ppm corresponding to the substitution in the benzene ring of **PhSOHPOH-2** sample.

$^{31}\text{P}$  MAS NMR spectra were also recorded for these samples (see Fig. 4). These spectra display only two signals at  $\delta = 32.5$  and 22.6 ppm, indicative of formation of two different phosphorus environments, such as phosphonate ( $-\text{P}=\text{O}$ ) group and phosphonic acid ( $-\text{P}-\text{O}-$ ),

**Table 1**

Textural parameters and amount of functional groups on the obtained mesoporous samples surface.

Sample	Functional groups	$S_{\text{BET}}$ , $\text{m}^2/\text{g}$	$V_s$ , $\text{cm}^3/\text{g}$	${}^1\text{d}_{\text{m}}$ , nm	${}^2\text{d}_{\text{m}}$ , nm	${}^3\text{d}_{\text{m}}$ , nm	$h_w$ , nm	$C_{\text{L}}$ , $\text{mmol}\cdot\text{g}^{-1}$	
								Theor.	Exper.
								$-\text{SO}_3\text{H}/-\text{PO}_3\text{H}_2$	$-\text{SO}_3\text{H}/-\text{PO}_3\text{H}_2$
<i>Ph</i>	$-\text{C}_6\text{H}_5$	663	0.67	5.6	6.0	9.0	2.1	1.6	ND
<i>PhP</i>	$-\text{C}_6\text{H}_5/\text{P}(\text{O})(\text{OEt})_2$	595	0.63	3.7	8.5	7.7	1.9	1.1/1.1	ND
<i>PhPOH-1</i>	$-\text{C}_6\text{H}_5/\text{P}(\text{O})(\text{OH})_2$	395	0.34	3.7	4.5	6.8	3.1	1.3/1.2	ND/0.72
<i>PhPOH-2</i>	$-\text{C}_6\text{H}_5/\text{P}(\text{O})(\text{OH})_2$	543	0.50	3.7	4.5	7.4	2.3	1.3/1.2	ND/0.75
<i>PhSOH</i>	$-\text{C}_6\text{H}_5/\text{SO}_3\text{H}$	551	0.65	5.6	7.5	10.5	2.5	1.3/1.2	0.62
<i>PhSOHPOH-1</i>	$-\text{C}_6\text{H}_5/\text{SO}_3\text{H}/-\text{PO}_3\text{H}_2$	313	0.37	4.6	7.5	ND	ND	1.3/1.2	0.71/1.25
<i>PhSOHPOH-2</i>	$-\text{C}_6\text{H}_5/\text{SO}_3\text{H}/-\text{PO}_3\text{H}_2$	420	0.56	4.7	7.5	ND	ND	1.3/1.2	0.63/1.45
<i>SHSOH</i> [39]	$-\text{SH}/\text{SO}_3\text{H}$	420	0.55	6.5	ND	8.0	2.3	0.2/0.6	0.44/0.17
<i>VPhSOH</i> [40]	$-\text{C}_6\text{H}_5/\text{SO}_3\text{H}$	500	ND	6.0	ND	ND	ND	10.9 (C, %)	0.70
<i>SiO<sub>2</sub>SOH</i> [41]	$-\text{SO}_3\text{H}$	500	ND	ND	ND	ND	ND	0.45	0.47

Notes: 1 – from N<sub>2</sub> desorption isotherms, 2 – from TEM images, 3 – from XRD data,  $h_w$  – wide of the pore wall, ND – not determined.**Fig. 4.**  ${}^{29}\text{Si}$  MAS,  ${}^{31}\text{P}$  MAS and  ${}^{13}\text{C}$  CP MAS NMR spectra of the PhPOH-2 and PhSOHPOH-2 samples.

respectively.

${}^1\text{H}$  MAS NMR spectra of obtained silica samples, contain three main contributing peak lines at 1.0, 3.7, and 5.7 ppm (Fig. S3). The peak at 1.0 ppm is assigned to the both CH<sub>2</sub> of alkyl chain (Si-CH<sub>2</sub>-) and isolated silanol groups at the surface. Note that no peak could be observed at their usual position around 1.8 ppm in the spectrum of pristine silica. It is known, however, that protons in isolated silanol groups also produce

lines between 0.5 and 1.5 ppm. Chemical shift at 3.7 ppm is assigned to the CH<sub>2</sub> of aliphatic chains and hydrogen-bonded silanols. At the same time lines at 5.9 ppm were assigned to weakly bound, relatively mobile adsorbed water and other hydrogen-bonded groups display a peak in this region contributing to the total intensity. The latter peaks (7.1 and 7.7 ppm) attributed to the aromatic rings on the surface, in agreement with bifunctional mode of bonding observed by  ${}^1\text{H} \rightarrow {}^{13}\text{C}$  CP-MAS NMR.

Potentiometric titration was applied to determine concentration of functional groups in the obtained mesoporous samples (Fig. 5). It has been widely used to quantify the amount of acidic and basic surface groups in functional materials [25] and has been employed to get information about the amount of specific groups in the initial and modified polyfunctional mesoporous materials (Table 1). The processed titration curves are shown in Figs. S4 and S5. Different numbers of endpoints were observed in various materials. For instance, the titration curve of the *VPhSOH*, *PhSOHPOH-1* and *PhSOHPOH-2* samples exhibited two endpoints, which divided the curve into three regions: neutralization of sulfonic acid groups, neutralization of phosphonic acid groups and then of weak phenolic acid groups (Fig. 5). The amounts of the specific functional groups in the materials were calculated from the amounts of NaOH titrated in each stage (Figs. S4 and S5), from left to right, and are summarized in Table 1.

The chemical characteristics of the initial and corresponding derivative samples listed in Table 1 indicate that there are significant differences in the surface concentrations of the theoretical values calculated from amounts of components in synthesis mixtures and amounts of functional groups determined by potentiometric method. Additionally, the concentration of sulfonic groups is high enough after sulfonation, but not all phenyl groups were transferred into phenylsulfonic groups (Table 1). Interestingly, amounts of primary phosphonic groups determined in the pristine *PhPOH-1* and *PhPOH-2* samples were retained after sulfonation reaction (*PhSOHPOH-1* and *PhSOHPOH-2*), while larger amounts of phenylsulfonic groups were observed in solids after reaction. This could be attributed to the fact that the phenyl groups reacting with ClSO<sub>3</sub>H were successfully converted into stable phenylsulfonic groups (Table 1).

Thermogravimetric analyses were carried out to determine the thermal stability and content of organic matter in the silica samples. As shown in Fig. S6, the weight loss of about 8 wt% from room temperature to 125 °C was due to desorption of physically adsorbed water and solvents. Weight loss of almost 24 wt % from 135 °C to 600 °C could be mostly corresponding to the decomposition of various organic functional groups. The weight loss at higher temperatures is proportional to the concentration of the introduced functional groups, which is reflected by a peak on the DTG curves in the range of temperatures between 300 °C and 650 °C. The decomposition of organic groups in the aforementioned temperature range is reflected by 13% weight loss for the sample *PhPOH-2* (1.1 mmol·g<sup>-1</sup>), and about 10% weight loss for the sample *PhPOH-1* (1.0 mmol·g<sup>-1</sup>). Note also that the total weight loss for the first sample was larger than that for the second one. This could be providing evidence that one-pot reaction allows achieving the higher concentration of functional groups, because post-treatment with

hydrochloric acid might remove some organic groups from the mesostructured surface of the sample (Fig. S6).

The next section is divided into two parts. The adsorption properties of obtained materials toward Ce(III) ions are discussed first followed by the luminescence performance in Ce-incorporated solid samples.

### 3.3. Adsorption properties of mesoporous materials

It is known that the adsorption capacity can affect the luminescence intensities of luminophores [42]. The adsorption capacity of the Ce-containing materials was verified by ICP analysis of the amount remaining concentration metal in the solution after doping stage (Table 2).

The adsorption capacities of obtained mesoporous samples for Ce(III) ions increased in the order *SBA-15* < *SiO<sub>2</sub>SOH* < *Ph* < *SHSOH* < *PhSOHPOH-2* < *PhSOH* < *PhSOHPOH-1* (Table 2). The adsorption performance of non-functionalized *SBA-15* for Ce(III) ions adsorption is the worst in the test adsorbents, despite the large surface areas (as denoted by N<sub>2</sub> adsorption/desorption experiment, Fig. 3) and the presence of exposed isolated silanol groups on the surface of SBA-15 matrix (as indicated by FTIR analysis in Fig. S2). It is well-known that Ce(III) ions (like other REEs), readily form complexes with O-donor ligand [43]. The silanol group on the surface of SBA-15 may serve as an O-donor ligand for complexation with Ce(III) ions, thus leading to a reasonable Ce(III) adsorption ( $\equiv\text{Si-OH} + \text{Ce}^{3+} \rightarrow \equiv\text{Si-O-Ce}^{2+} + \text{H}^+$ ).

However, for phenyl-containing of the SBA-15 matrix, the Ce(III) uptake increased unexpectedly (Table 2), indicating most probably the availability of the phenolic groups and their interaction with Ce(III) ions. We assume that the adsorption of Ce(III) on *Ph* sample occurs not

**Table 2**

Results of Ce(III) ions incorporation of the initial and organofunctional mesoporous samples.

Sample	Functional groups	C <sub>0</sub> , mol·dm <sup>-3</sup>	q <sub>e</sub> , mg·g <sup>-1</sup>	q <sub>e</sub> , mmol·g <sup>-1</sup>
<i>SiO<sub>2</sub>SOH</i> [41]	-SO <sub>3</sub> H	0.101	71.11	0.51
<i>SHSOH</i> [39]	-SH/-SO <sub>3</sub> H	0.101	141.89	1.01
<i>SBA-15</i>	-OH	0.097	57.60	0.41
<i>Ph</i>	-C <sub>6</sub> H <sub>5</sub>	0.097	88.02	0.63
<i>PhSOH</i>	-C <sub>6</sub> H <sub>5</sub> /-SO <sub>3</sub> H	0.097	237.05	1.69
<i>PhSOHPOH-</i> 1	-C <sub>6</sub> H <sub>5</sub> /-SO <sub>3</sub> H/- PO <sub>3</sub> H <sub>2</sub>	0.097	259.19	1.85
<i>PhSOHPOH-</i> 2		0.097	175.12	1.25

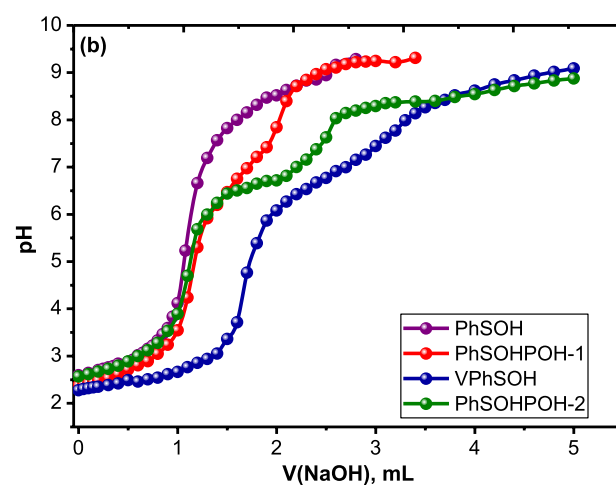
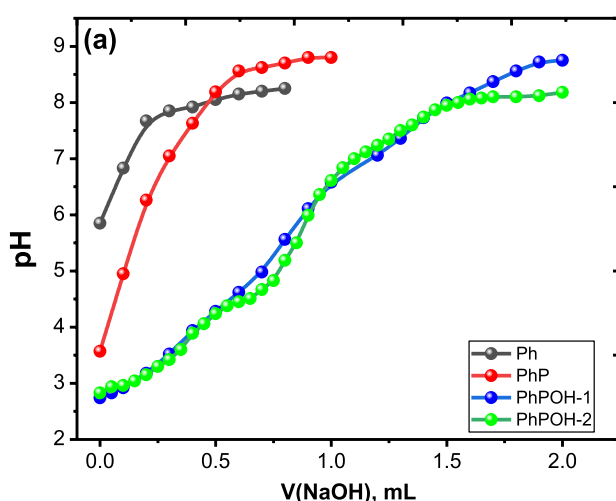


**Fig. 5.** pH titration curves for the initial mesoporous silica (a) and the corresponding derivatized materials (b).

only due to electrostatic interaction but also due to phenolic groups, which form under the synthesis conditions ( $\equiv\text{Si}-\text{PhOH} + \text{Ce}^{3+} \rightarrow \equiv\text{Si}-\text{PhO}\text{Ce}^{2+} + \text{H}^+$ ). The presence of the latter was confirmed by the potentiometric titration of the samples (Fig. 5). Another observed feature is that increasing the coverage with mono- (*SiO<sub>2</sub>SOH* sample) and bi-functional (*SHSOH* sample) aliphatic sulfonic groups on the surface of the material does benefit the Ce(III) sorption, which suggests that sulfonic group is the main binding group for Ce(III) ions ( $\equiv\text{Si} \sim \text{SO}_3\text{H} + \text{Ce}^{3+} \rightarrow \equiv\text{Si} \sim \text{SO}_3\text{Ce}^{2+} + \text{H}^+$ ).

Finally, the high uptake of Ce(III) ions was achieved for bifunctional samples with various combination of S,P,O-donor ligands (Table 2). When the mesoporous silica was modified by phenylsulfonic groups (*PhSOH*), the Ce(III) uptake reached 237 mg·g<sup>-1</sup>(1.69 mmol·g<sup>-1</sup>), a value four times larger than that of unmodified **SBA-15**. This may be attributed to the high concentration of ion-exchange sulfonic groups and larger surface area combined with pore availability (Table 1). Taken together, it is seen that sulfonic group is an effective ligand for Ce(III), and the weak acidic (including silanol) groups as well as benzene ring on the surface of *PhSOH* and *Ph* give low contribution to the Ce(III) uptake. This result firmly proves that the performance in the Ce(III) ions adsorption is significantly improved by introducing of the phenylsulfonic groups.

Change in the structure of *PhSOH* sample upon the Ce loading was followed by FTIR study of Ce-incorporated *PhSOH* sample (Fig. 6).

IR spectrum of Ce-incorporated silica exhibited a typical pattern of silica bands (Fig. S2 and Fig. 6). For Ce-containing sample spectrum the disappearance of the band the isolated silanol groups (Si-OH) at 3750 cm<sup>-1</sup> due to insertion of Ce(III) ions into silica matrix. This is an indication of the interaction between silanol groups and Ce (III) ions. Another fact is that the presence of Ce(III) ions significantly increased intensity of sharp adsorption bands in the range of 3200–3400 cm<sup>-1</sup> and 1600–1620 cm<sup>-1</sup>, which suggests that H<sub>2</sub>O molecules constitute one of main complexation ligands. The change in intensity of the S-O bands (1190 cm<sup>-1</sup>) of Ce-incorporated sample was attributed to ion-exchange

bonding between Ce(III) ions and sulfonic groups of *PhSOH* sample. On the other hand, the shift of C=C band at around 1465 cm<sup>-1</sup> is indicating involvement of benzene ring in complexation reaction with Ce(III) ions. Thus, the phenylsulfonic groups on the *PhSOH* silica surface contribute strongly to Ce(III) incorporation (see Table 2).

Moreover, the major improvement of Ce(III) adsorption is further enhanced after co-modification by phosphonic and phenylsulfonic groups (*PhSOHPOH-1* and *PhSOHPOH-2* samples), i.e. are large (Table 2). This is an expected result. The complexation mechanism of REEs incorporation on P,O-containing groups on the solids is predominant in this case [44]. The increased adsorption capacity of polyfunctional samples (*PhSOHPOH-1* and *PhSOHPOH-2*) compared to the samples containing only phenylsulfonic groups (*PhSOH*), is probably through high amount of functional groups.

The stoichiometry of the complexes formed between cerium(III) and organofunctional groups was evaluated based on amount of functional groups (Table 1) and adsorption capacity (Table 2) of the sample. For example, *PhSOHPOH-1* sample (dried at 60 °C) has the ratio of C<sub>L</sub>: q<sub>e</sub> = 1.96 : 1.85, which indicates the formation of 1:1 stoichiometry complexes shows a clear 1:1 stoichiometry complex. This stoichiometry shows that in addition to the divalent -PO<sub>3</sub>H<sub>2</sub> and monovalent -SO<sub>3</sub>H groups, the Ce(III) ion would require another anion as summarized by the Scheme 3. In the absence of Cl<sup>-</sup> anions, central ions may be coordinated with this stoichiometry suggests a coordinated hydroxyl groups or water molecules.

Significant difference in adsorption properties for of *PhSOHPOH-2* sample was observed. It was deduced that the ratio C<sub>L</sub>: q<sub>e</sub> = 2.07 : 1.25, which shows predominate of complexes with stoichiometry 1:2. Based on the above description, the functional groups on the surface sample should locate like clusters inside the channels rather than other places. Besides, coordination number of REEs in complexes can be achieved through the employment of multidentate ligands, as these provide multiple donor atoms such as phosphonic groups that block coordination sites [43]. It is conclusive that the distributions of Ce(III) ions into

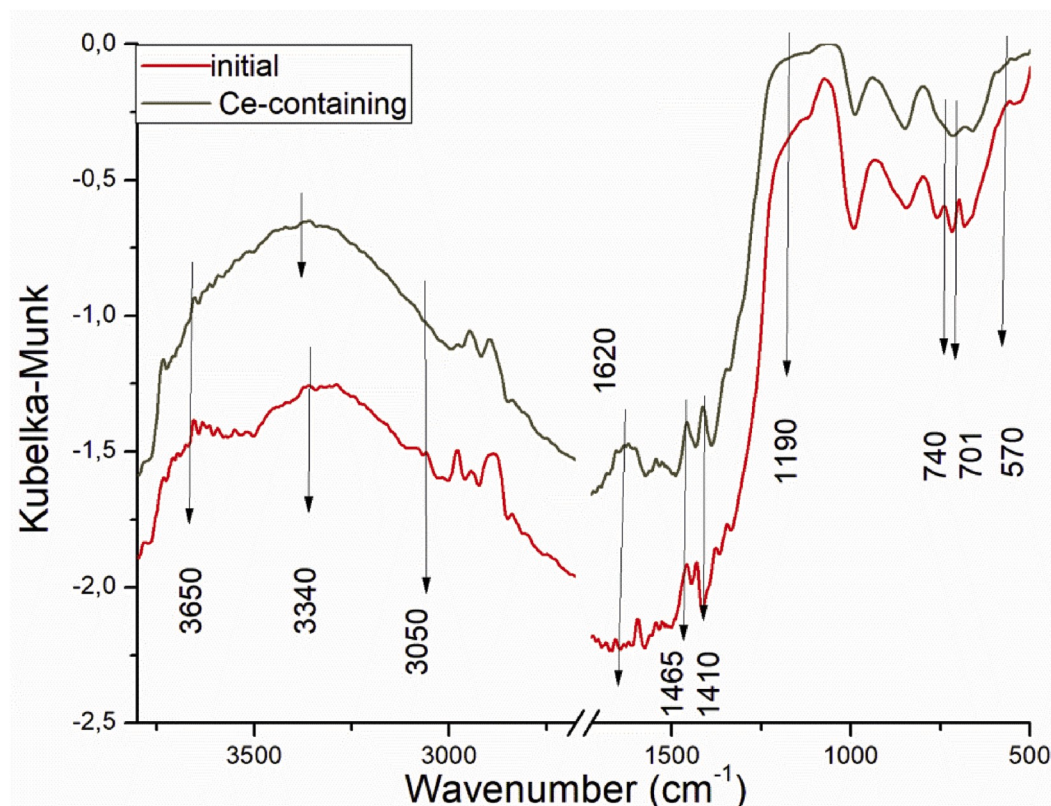
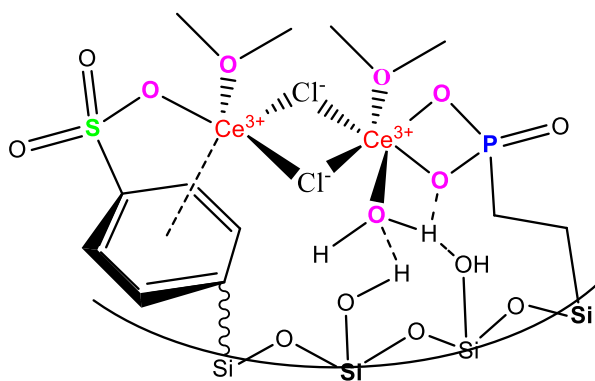


Fig. 6. FTIR spectra in Kubelka-Munk coordinate of initial and Ce-incorporated *PhSOH* samples.



**Schema 3.** Possible structure of the Ce(III)-incorporated chromophore for **PhSOHPOH-1** sample.

mesopores of **PhSOHPOH-2** sample are irregular. According to the foregoing results, it is found that direct addition of the prehydrolysis DPTS into the reaction mixture in synthesis of bifunctional SBA-15 with phosphonic and phenyl groups promotes the cluster formation of functional groups.

#### 3.4. Photoluminescence properties of Ce(III)-incorporated silica samples

It is known that the cerium(III) luminescence quenches on the silica centers [21]. The luminescence spectra were measured to get more information about optical behavior of both the Ce(III)-incorporated bare and organofunctional mesoporous samples. The emission features were compared for different mesoporous matrices revealing emission peak of high intensity for unequivocal identification of Ce(III)-incorporation into silica materials.

##### 3.4.1. Undried Ce-incorporated mesoporous materials

The room temperature photoluminescence excitation and emission spectra of bare **SBA-15** and **PhSOH** samples were measured in solid powder state with the slit width of 0.7 nm with filter(x2) and without filter (Fig. 7).

Excitation at 246 nm by xenon lamp (150 W) permits to detect short-lived emission of Ce(III) maximized in the UV region between 350 and 390 nm, which may be assigned to the 4f→5d transitions of Ce(III) ions (Fig. 7a). Characteristic broad emission band of Ce(III) is detected with maximum around 375 nm under 295 nm excitation, but it is worth noting that the observed emission band is inhomogeneously broadened

because its excitation spectrum shows small low-energy shift when emission wavelength is set longer. This is rather typical situation for Ce (III) centers in a powder matrix environment, where little change in the short-distance order and eventual defects nearby shift the position of 5d level and/or change its relaxation pathway [30]. Thus, luminescence studies confirmed that cerium(III) had been incorporated into the mesoporous silica matrix.

The emission of triply charged cerium ions incorporated into **PhSOH** matrix occurs as a doublet band due to transitions from the relaxed lowest 5d excited state to the spin-orbit split 4f ground states ( $^2F_{5/2}$ ,  $^2F_{7/2}$ ). The energy between levels at the bands maxima is quite close. The presence of two types of bands in the photoluminescence spectra (Fig. 7b) can be related to the different environments of the Ce(III) ions in the silica matrix. A strong overlap of the activator 5d orbitals with ligand orbital causes high sensitivity of their spectral characteristics to the local structural environment. The luminescence intensity of the Ce-incorporated modified silica (Fig. 7b) indicates the multi-photon relaxation pathways arising from the surface coated by high vibrational energy molecules of the S-containing functional and silanol groups.

Photoluminescence study of the Ce-incorporated mesoporous samples series revealed the typical light emissions of the Ce(III) ions, but with varying intensity in response to nature and concentration of functional groups. The impact of adsorption capacity for Ce(III) ions and emission photoluminescence of pure mesoporous silica and series of organofunctional derivates dried at room temperature in air atmosphere under excitation at 246 nm was studied (Fig. 8).

The luminescence performance of non-functionalized **SBA-15** and **Ph** is the worst among the test materials (Fig. 8). It's obvious that the changes in the intensity photoluminescence are associated with this functional evolution in the mesoporous silica. The high emission effect was achieved for samples modified with sulfonic groups, increasing the intensity of photoluminescence effect correlated with adsorption capacity and concentration of functional groups similar to all the samples. It was observed that the Ce(III) ion showed a very strong photoluminescence intensity for **PhSOHPOH-1** and **PhSOHPOH-2** samples based on phosphonic and phenylsulfonic groups (Fig. 8). The increased luminescence intensity of polyfunctional samples (**PhSOHPOH-1** and **PhSOHPOH-2**) compared to the samples containing only phenylsulfonic groups (**PhSOH**), is probably because of their high sensitized luminescence effect of Ce(III) on silica surface through phosphonic groups. Though, when the amount of phosphonic and sulfonic groups increases significantly, possibly due to the heterogeneous distribution of groups and achievement of higher coordination number of Ce(III) ions along with the influence of numerous silanol groups, the adsorption capacity

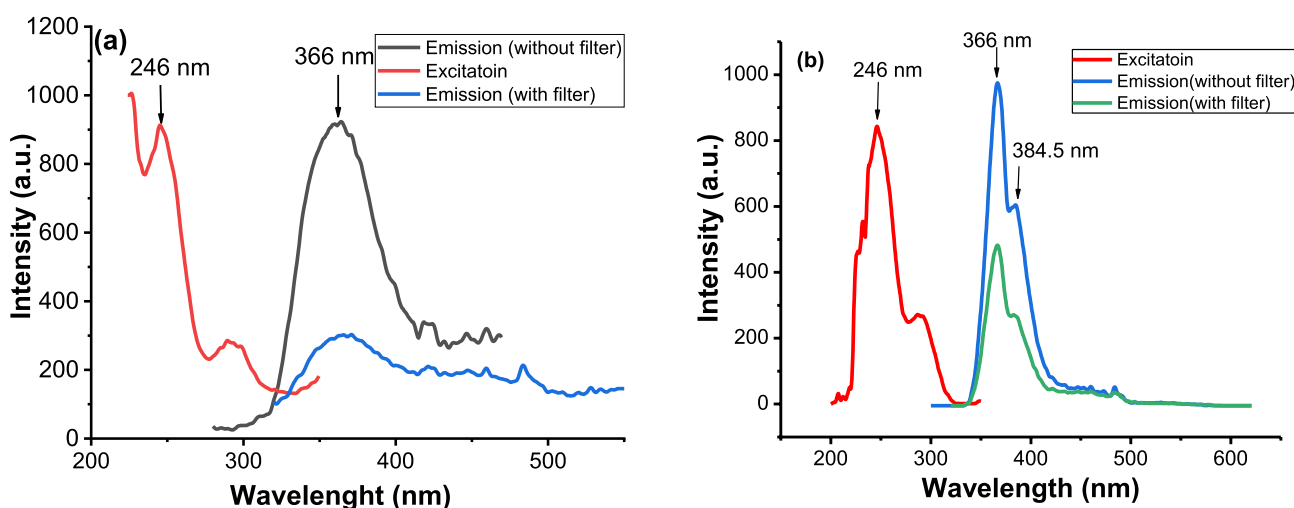


**Fig. 7.** Emission and excitation spectra of Ce-incorporated **SBA-15** (a) and **PhSOH** (b) samples dried at room temperature (Experim. conditions:  $V = 15 \text{ cm}^3$ , initial conc.  $C(\text{CeCl}_3) = 0.097 \text{ mol} \cdot \text{dm}^{-3}$ ,  $\text{pH} = 2.45$  (**SBA-15**) and  $\text{pH} = 1.67$  (**PhSOH**)).

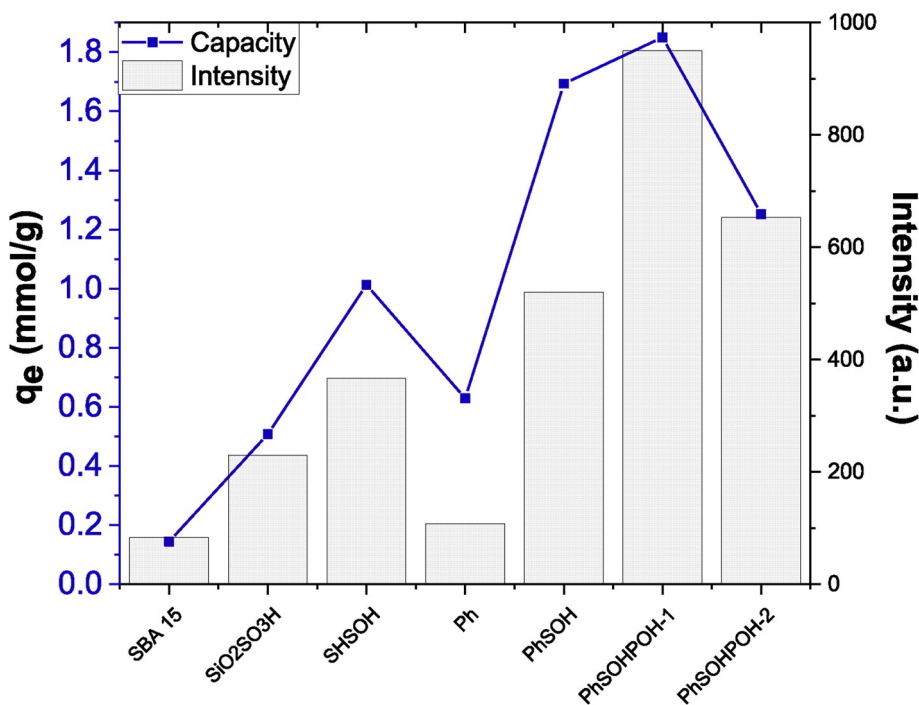


**Fig. 8.** Comparison of Ce(III) ions adsorption capacity and intensity photoluminescence spectra (with filter x4, 350 nm) of pristine and various functionalized silica under the same experimental conditions ( $m(\text{sorbent})/V(\text{solution}) = 0.4 \text{ mg cm}^{-3}$ ,  $[\text{Ce}] \text{ initial} = 0.1 \text{ mol dm}^{-3}$ ).

for Ce(III) and the luminescence intensity finally decrease (**PhSOHPOH-2** sample). However, high amount of functional groups on the surface of the **PhSOHPOH-2** sample should be responsible for another mechanism of Ce(III)-incorporation and as the result quenching the luminescence (Fig. S7). That is, the increase in the functional groups coverage does not benefit the Ce(III) uptake, whereas the drop of the phosphonic groups brings negative effects on the Ce(III) uptake. Thus, the **PhSOHPOH-1**

sample demonstrates excellent luminescence properties (dominant emission transition in the purple region at 366 nm), indicates possibility to be used in optical detection, labeling, etc.

The effect of the concentration of Ce(III) ions over the range of 0.1–1 mol·dm<sup>-3</sup> was further studied (Fig. 9). The fluorescence intensity was increased with Ce(III) concentration in the range of 0.01–0.1 M without quenching effect (decrease in luminescence intensity).

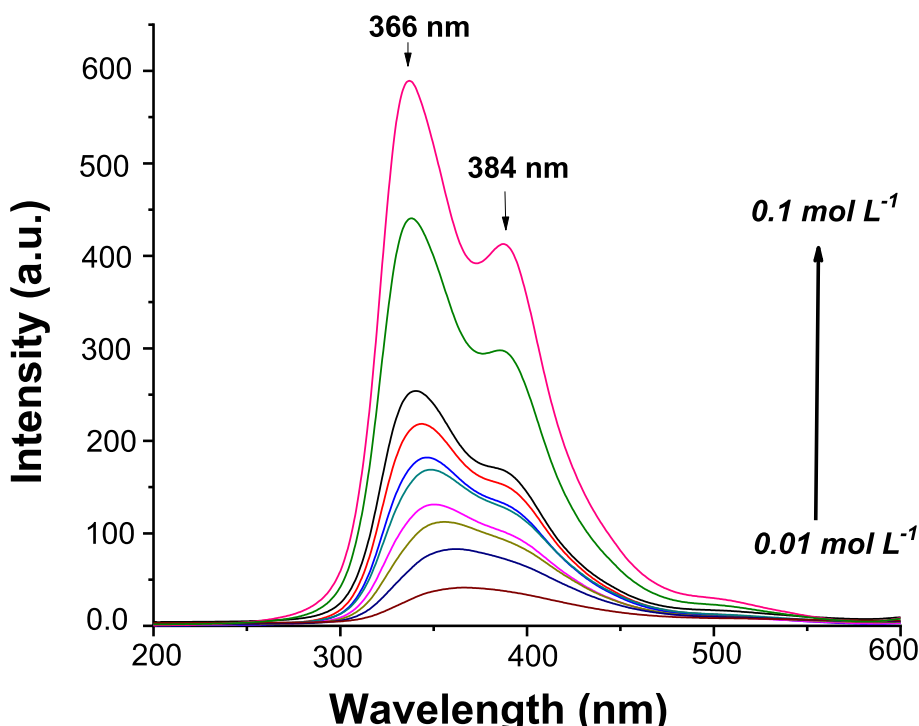


**Fig. 9.** Emission (smoothed) spectra of Ce-incorporated PhSOHPOH-1 sample (vs. concentration of Ce(III)) dried at room temperature. (Experimental conditions:  $\lambda_{\text{ex}} = 252 \text{ nm}$ ,  $C(\text{Ce(III)}) = 0.01\text{--}0.1 \text{ mol}\cdot\text{dm}^{-3}$ ,  $\text{pH} = 1.5\text{--}2.0$ , with filter x4, 350 nm).

**Fig. 9** shows the variation of shapes in luminescence spectra with different Ce(III) ion concentrations. The emission spectra were excited at 246 nm. The luminescence spectra depict increasing intensity emission as the concentration of the active REE increases in the silica matrix. The emission spectra of samples with high concentration of Ce(III) dried in the air atmosphere show two bands at 366 nm and 384 nm. At low concentrations of Ce(III), these two bands merge into an asymmetric broad band because of the large spatial extension of the 5d wave function and its interaction with lattice vibrations. At high concentration of Ce(III) ions may form a different complexes with functional groups of surface, and may thus change the luminescence effect with emergence of a broad structure band with two maxima at 366 nm and 384 nm. In general, the samples prepared with concentration of cerium(III) in solution near 0.1 M are expected to transfer energy from metal ions to complexes with other structural and activation centers.

### 3.4.2. Dehydrated Ce-incorporated materials

To verify the intramolecular energy transfer from the triplet state of the organic ligand to the resonance level of rare earth ion, the luminescence spectrum of the bare **SBA-15**, aliphatic ligand **SHSO<sub>3</sub>H** and **SiO<sub>2</sub>SO<sub>3</sub>H** were measured under irradiation of 246, 254 and 290 nm, with slit widths of 5 nm dried in the vacuum at 110 °C (**Fig. 10**).

Photoluminescence spectra of the Ce(III) incorporated in **SBA-15**

matrix after drying in vacuum revealed no specific emission for Ce(III) (**Fig. 10a**). The spectra showed only a wide minor emission peak between 350 and 500 nm. At the same time, UV-stimulated emission spectra were observed for **SHSOH** samples as asymmetric bands at 366 and 390 nm, as shown in **Fig. 10b**. Emission intensities of the sample excited by the short UV wavelengths are comparable, and in addition, the 246, 254 and 290 nm excitation of **SHSOH** gives rise to the same two emission bands with proportionally decreased intensity. These data show structure-sensitivity of luminescence to the coordination and structure of Ce-complex that is attributed to the excited state 5d and lack thereof for the ground state 4f. As mentioned above, the luminescence from Ce(III) ions is greatly affected by the local environment. When the samples were annealed in vacuum at 110 °C, a continuous densification process occurred (**Fig. 10a**). Thus, we suggest that the change in the fluorescence from the Ce(III)-incorporated silica is associated with aggregation together of Ce(III) ions in pores after the water removal by drying. The similar process was first observed in a Ce-containing silica prepared by sol-gel [45]. As for hydrophilic **SHSOH** solids (**Fig. 10b**), mesoporous silica matrix can easily adsorb atmospheric water into its pores when exposed to air. Thus, the Ce(III) ions located within the pores coordinate to the adsorbed and residual water, and the terminal OH- and S-containing two types of groups of the silica units. This results in luminescence spectra with two intensive bands. In fact, when **SHSOH**

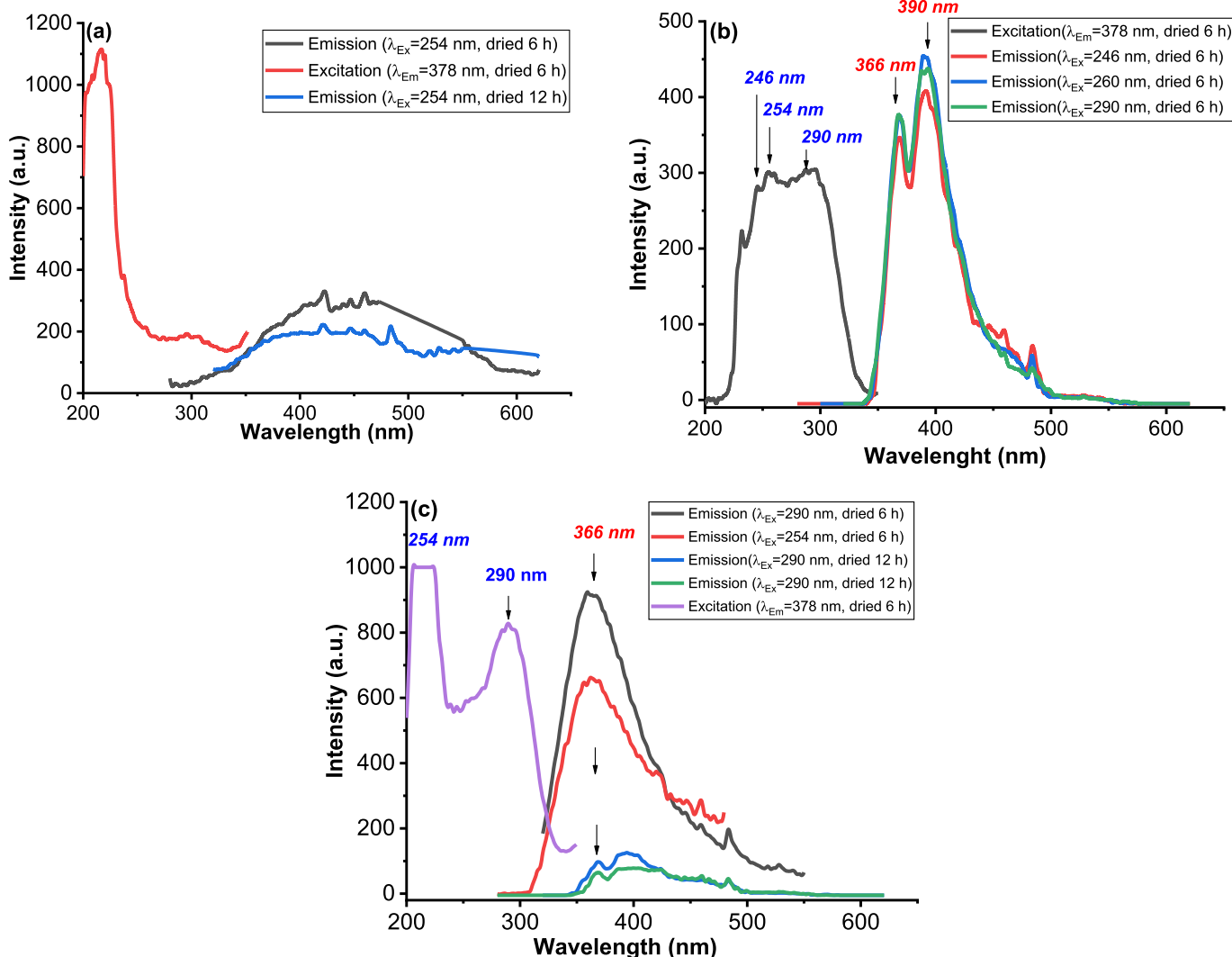


**Fig. 10.** Emission and excitation spectra (without filter) of Ce-incorporated **SBA-15** (a), **SHSOH** (b) and **SiO<sub>2</sub>SOH** (c) sample dried in the vacuum at 110 °C (Experimental conditions: C(Ce(III)) = 0.1 mol·dm<sup>-3</sup>, pH = 1.5–2.0).

and  $\text{SiO}_2\text{SOH}$  samples were exposed to air for longer time, the luminescence was enhanced due to the decrease of concentration quenching effect. Annealing will evidently increase the  $\text{Ce}^{3+}$  concentration in the liquid through the removal of water, and thus result in an increase in the degree of concentration quenching. Such an increase is thought to reduce the emission intensity with the drying until 12 h at 110 °C. In the meantime, the Ce(III) ions become gradually coordinated with functional and silanol groups. The coupling with the vibration of the terminal OH-groups reduces the radiative efficiency due to non-radiative relaxation. In other words, the concentration quenching effect and the coordination of Ce(III) ions with O- and S-containing groups may altogether reduce the emission intensity to the minimum after about 12 h drying in vacuum (110 °C).

In addition, the low emission peaks of Ce-incorporated  $\text{SiO}_2\text{SOH}$  sample appeared at 366 nm (Fig. 910). The excitation spectrum showed two peaks at 254 and 290 nm. The  $\text{SiO}_2\text{SOH}$  sample still maintained non-excellent luminescent properties even after 12 h dried in vacuum (Fig. 10c). We suggest that the removal of the OH-groups decreases the photoluminescence in two ways. First, the decrease in the number of Ce(III) ions coordinated with the residual silanol groups. Second, the decrease in the number of binding O-containing groups will contribute to the coordination of Ce(III) ions with functional groups and so disperse Ce(III) ions, which increases the degree of concentration quenching. This may also contribute to the decreased peak shift with increasing dried time.

#### 4. Conclusions

The series of polyfunctional mesoporous silicas acting as ‘support for luminophores’ were successfully synthesized via template approach introducing various organosilanes and sodium silicate as a structuring agent at the same time. Mesoporous SBA-15 silicas containing phenyl and ethylphosphonic groups were sulfonated and hydrolyzed, respectively, to produce acid groups on the surface of the pores. The comparative investigation of textural and composition characteristics of silica with regard to surface concentration of the groups allowed us to get information about the surface chemistry of the obtained silicas. The photoluminescence properties of Ce(III) ions in various mesoporous silicas modified by phenyl/aliphatic sulfonic and phosphonic groups were investigated in order to optimize these for potential utilization as Ce(III) quantum cutting material. Utilizing SBA-15-based mesoporous material containing phenylsulfonic groups increased the capacity towards Ce(III) ions. This may be because of the high acidity and ion-exchange properties in this material when compared to that of bare SBA-15 with the same or even larger specific area. The mesopores preserved adsorption capacity for Ce(III) ions up to  $1.85 \text{ mmol}\cdot\text{g}^{-1}$ , indicating the high effective interaction of metal ions with functional groups. The photoluminescence properties of Ce-incorporated polyfunctionalized silica frameworks were investigated. Therefore, the higher luminescence intensity in bifunctional mesoporous samples (phenylsulfonic and phosphonic groups) compared to monofunctional aliphatic and aryl-containing sulfonic groups can be explained by the differences in the Ce(III) complexes structures of these materials with and sensitization effect of phosphonic groups. Such synergistic effect of Ce(III) loading is related to the concentration of sulfonic groups, presence of phosphonic groups as well as phenyl groups and it is not dependent on the pore sizes and surface area of silica material.

#### Declaration of competing interest

The authors declare that they have no known competing financial interests or personal relationships that could have appeared to influence the work reported in this paper.

#### CRediT authorship contribution statement

**Natalia G. Kobylinska:** Methodology, Formal analysis, Investigation, Writing - original draft. **Oksana A. Dudarko:** Conceptualization, Methodology, Formal analysis, Investigation, Writing - original draft, Writing - review & editing. **Inna V. Melnyk:** Writing - review & editing, Project administration. **Gulaim A. Seisenbaeva:** Supervision, Validation, Funding acquisition. **Vadim G. Kessler:** Writing - review & editing, Resources, Funding acquisition.

#### Acknowledgment

Authors thank for the financial support of the joint Ukrainian-Lithuanian research project M/8–2019 and project “Multifunctional hybrid adsorbents for water purification” supported by the Swedish Research Council (Vetenskapsrådet) Swedish Research Program Links Dnr. 2018–2021. The authors are also indebted to the EU ERA-MIN 2 Program for support of the MetRecycle project (via Vinnova Swedish Research Council grant No. 2018-00739).

#### Appendix A. Supplementary data

Supplementary data to this article can be found online at <https://doi.org/10.1016/j.micromeso.2020.110331>.

#### References

- [1] J.-C.G. Bünzli, C. Piguet, Chem. Soc. Rev. 34 (2005) 1048–1077, <https://doi.org/10.1039/b406082m>.
- [2] K. Matsumoto, J.G. Yuan, A. Sigel, H. Sigel (Eds.), *Metal Ions in Biological Systems*, Marcel Dekker Inc., New York, 2003, pp. 191–232.
- [3] S. Faulkner, S.J.A. Pope, B.P. Burton-Pye, Appl. Spectrosc. Rev. 40 (2005) 1–31. <https://doi.org/10.1081/ASR-200038308>.
- [4] L. Ozawa, M. Itoh, Chem. Rev. 103 (2003) 3835–3856, <https://doi.org/10.1021/cr0203490>.
- [5] M.J. Weber, K.A. Gschneider Jr., E.L. Eyring (Eds.), *Handbook on the Physics and Chemistry of the Rare Earths*, North-Holland, Amsterdam, 1979.
- [6] V.R. Kharabel, S.J. Dhoble, S.V. Moharil, J. Phys. D Appl. Phys. 41 (2008) 205413–205419, <https://doi.org/10.1088/0022-3727/41/20/205413>.
- [7] A.J. Silversmith, N.T.T. Nguyen, B.W. Sullivan, D.M. Boye, C. Ortiz, K.R. Hoffman, J. Lumin. 128 (2008) 931–933. <https://doi.org/10.1016/j.jlumin.2007.11.049>.
- [8] M. Moszynski, T. Ludziejewski, D. Wolski, W. Klamra, L.O. Norlin, Nucl. Instrum. Methods 345 (1994) 461–467, [https://doi.org/10.1016/0168-9002\(94\)90500-2](https://doi.org/10.1016/0168-9002(94)90500-2).
- [9] M. Alshourbagy, S. Bigotta, D. Herbert, A. Del Guerra, A. Toncelli, M. Tonelli, J. Cryst. Growth 303 (2007) 500–505, <https://doi.org/10.1016/j.jcrysgro.2007.01.024>.
- [10] B. Liu, Ch. Shi, M. Yin, Y. Fu, G. Zhang, G. Ren, J. Lumin. 117 (2006) 129–134, <https://doi.org/10.1016/j.jlumin.2005.04.013>.
- [11] C. Dujaudin, C. Mancini, D. Amans, G. Ledoux, D. Abler, E. Auffray, J. Appl. Phys. 108 (2010) 13510–13517, <https://doi.org/10.1063/1.3452358>.
- [12] C.W. Jia, E.Q. Xie, A.H. Peng, R. Jiang, F. Ye, H.F. Lin, T. Xu, Thin Solid Films 496 (2006) 555–559, <https://doi.org/10.1016/j.tsf.2005.08.378>.
- [13] H. Yu, D.M. Jiang, Q.Z. Zhai, W.H. Hu, L. Fan, J. Lumin. 132 (2012) 474–477, <https://doi.org/10.1016/j.jlumin.2011.08.044>.
- [14] A. Veda, A. Baraldi, C. Canevali, R. Capelletti, N. Chiodini, R. Francini, M. Martini, F. Morazzoni, M. Nikl, R. Scotti, G. Spinolo, Nucl. Instrum. Methods A 486 (2002) 259–263, [https://doi.org/10.1016/S0168-9002\(02\)00713-1](https://doi.org/10.1016/S0168-9002(02)00713-1).
- [15] K. Binnemans, Chem. Rev. 109 (2009) 4283–4374, <https://doi.org/10.1021/cr8003983>.
- [16] E.R. Rand, M.B. Smuckler, E. Go, M.S. Bradley, J.W. Bruno, Inorg. Chim. Acta. 233 (1995) 71, [https://doi.org/10.1016/0020-1693\(94\)04448-5](https://doi.org/10.1016/0020-1693(94)04448-5).
- [17] W. Cai, Y. Zhang, L. Zhang, J. Phys. Condens. Matter 10 (1998) L473, <https://doi.org/10.1088/0953-8984/10/28/001>.
- [18] W. Cai, Y. Zhang, L. Zhang, J. Mater. Res. 14 (1999) 1922–1927, <https://doi.org/10.1557/JMR.1999.0258>.
- [19] G.Q. Xu, Z.X. Zheng, W.M. Tang, Y.C. Wu, J. Lumin. 126 (2007) 43–47, <https://doi.org/10.1016/j.jlumin.2006.05.001>.
- [20] H.J. Bi, W.P. Cai, H.Z. Shi, L.D. Zhang, B.D. Yao, J. Mater. Res. 15 (2000) 2364–2367, <https://doi.org/10.1557/JMR.2000.0340>.
- [21] R. Reisfeld, A. Patra, G. Panczer, M. Gaft, J. Optical Materials 13 (1999) 81–88, [https://doi.org/10.1016/S0925-3467\(99\)00015-4](https://doi.org/10.1016/S0925-3467(99)00015-4).
- [22] O.M. Ntwaeborwa, H.C. Swart, R.E. Kroon, P.H. Holloway, J.R. Botha, Surf. Interface Anal. 38 (2006) 458–461, <https://doi.org/10.1002/sia.2145>.
- [23] S.D. Topel, E.P. Legaria, C. Tiseanu, J. Rocha, J.-M. Nedelec, V.G. Kessler, G. A. Seisenbaeva, J. Nanoparticle Res. 16 (2014) 2783–2800, <https://doi.org/10.1007/s11051-014-2783-6>.
- [24] J. Liu, Q. Yang, M.P. Kapoor, N. Setoyama, S. Imagaki, J. Yang, L. Zhang, J. Phys. Chem. B 109 (2005) 12250–12256, <https://doi.org/10.1021/jp0509109>.

- [25] S. Inagaki, S. Guan, T. Ohsuna, O. Terasaki, *Nature* 416 (2002) 304–307, <https://doi.org/10.1038/416304a>.
- [26] Ch Shi, W. Wu, X. Bian, M. Pei, Sh Zhao, P. Chen, 34 (2016) 597–603. [https://doi.org/10.1016/S1002-0721\(16\)60067-4](https://doi.org/10.1016/S1002-0721(16)60067-4).
- [27] Y. Li, B. Yan, *Nanoscale Res. Lett.* 5 (2010) 701–708, <https://doi.org/10.1007/s11671-010-9534-0>.
- [28] L.F. Koao, H.C. Swart, R.I. Obed, F.B. Dejene, *J. Lumin.* 131 (2011) 1249–1254, <https://doi.org/10.1016/j.jlumin.2010.10.038>.
- [29] L.A. Goncharova, N.G. Kobylnska, M.E. Díaz-García, V.N. Zaitsev, *J. Anal. Chem.* 72 (2017) 724–733, <https://doi.org/10.1134/S106193481707005X>.
- [30] K. Klier, A.C. Miller, L.L. Zhang, M.K. Hatalis, *Chem. Mater.* 20 (2008) 1359–1366, <https://doi.org/10.1021/cm071754g>.
- [31] J. Wu, Zh Cui, Ch Zhao, H. Li, Ya Zhang, T. Fu, H. Naa, W. Xing, *Int. J. Hydrogen Energy* 34 (2009) 6740–6748, <https://doi.org/10.1016/j.ijhydene.2009.06.051>.
- [32] D. Zhao, Q. Huo, J. Feng, B.F. Chmelka, G.D. Stucky, *J. Am. Chem. Soc.* 120 (1998) 6024–6036, <https://doi.org/10.1021/ja974025i>.
- [33] O. Dudarko, Ch Gunathilake, V.V. Sliesarenko, Y.L. Zub, *Jaroniec Colloid Surf. A Physicochem. Eng. Asp.* 459 (2014) 4–10, <https://doi.org/10.1016/j.colsurfa.2014.06.036>.
- [34] X.-M. Wang, X.-Z. Du, C.-L. Li, X. Cao, *Appl. Surf. Sci.* 254 (2008) 3753–3757, <https://doi.org/10.1016/j.apsusc.2007.11.031>.
- [35] O. Dudarko, Y. Zub, *Chem. J. Mold. Gen. Industr. Ecolog. Chem.* 12 (2) (2017) 79–86.
- [36] E.P. Barrett, L.G. Joyner, P.P. Halenda, *J. Am. Chem. Soc.* 73 (1951) 373–380, <https://doi.org/10.1021/ja01145a126>.
- [37] A. Dabrowski, M. Barchak, O.A. Dudarko, YuL. Zub, *Pol. J. Chem.* 81 (2007) 475–483.
- [38] M. Thommes, K. Kaneko, A.V. Neimark, J.P. Olivier, F. Rodríguez-Reinoso, J. Rouquerol, K.S.W. Sing, *Pure Appl. Chem.* 87 (2015) 1051–1069, <https://doi.org/10.1515/pac-2014-1117>.
- [39] O.A. Dudarko, S. Barany, *RSC Adv.* 8 (2018) 37441–37450. <https://doi.org/10.1039/C8RA07119E>.
- [40] Agilent bond Elut silica-based SPE selection guide. <https://www.agilent.com/cs/library/selectionguide/public/5990-8591EN.pdf>.
- [41] V.N. Zaitsev, N.G. Kobylnskaya, L.S. Kostenko, V.I. Gerda, *J. Anal. Chem.* 63 (2018) 779–786, <https://doi.org/10.1134/S1061934808080121>.
- [42] J.R. Lakowicz, *Principles of Fluorescence Spectroscopy*, third ed., Springer, New York, USA, 2006.
- [43] F. Ortú, D.P. Mills, *Handb. Phys. Chem. Rare Earths* 55 (2019) 1–87.
- [44] L. Kostenko, N. Kobylnska, S. Khainakov, S. García Granda, *Microchim. Acta* 186 (2019) 474–490, <https://doi.org/10.1007/s00604-019-3520-8>.
- [45] H. Bi, W. Cai, H. Shi, B. Yao, L. Zhang, D. Phy, *Appl. Phys.* 33 (2000) 2369–2372, <https://doi.org/10.1088/0022-3727/33/19/304>.